Transport spectroscopy in a time-modulated open quantum dot

C. S. Tang,[1] Y. H. Tan,[2] and C. S. Chu[2]
[1]*Physics Division, National Center for Theoretical Sciences, P.O. Box 2-131, Hsinchu 30013, Taiwan, Republic of China*
[2]*Department of Electrophysics, National Chiao-Tung University, Hsinchu 30010, Taiwan, Republic of China*
(Received 2 October 2002; published 30 May 2003)

We have investigated the time-modulated coherent quantum transport phenomenon in a ballistic open quantum dot. Conductance G and the electron dwell time in the dots are calculated by a time-dependent mode-matching method. Under high-frequency modulation, the traversing electrons are found to exhibit three types of resonant scatterings. They are intersideband scatterings into quasibound states in the dots, into true bound states in the dots, and into quasibound states just beneath the subband threshold in the leads. Dip structures or fano structures in G are their signatures. Our results show structures due to $2\hbar\omega$ intersideband processes. At the above scattering resonances, we have estimated, according to our dwell time calculation, the number of round-trip scatterings which the traversing electrons undertake between the two dot openings.

DOI: 10.1103/PhysRevB.67.205324 PACS number(s): 73.23.−b, 72.30.+q , 72.10.−d

I. INTRODUCTION

In the past decade, the quantum transport phenomenon in open quantum dots has received much attention.[1–11] The open quantum dot, consisting of a submicron sized cavity connecting via point contact leads to two end-electrodes, has become an important device for the investigation of phase-coherent processes and their various mechanisms. The size of the dot and the width of the leads can be controlled by split gates. In high electron mobility samples, and at sufficient low temperatures, the phase-coherent length may well exceed the dimension of the device, allowing electrons to remain coherent while traversing the dot.

Meanwhile, there has been growing interest in the high-frequency responses of mesoscopic nanostructures. The time-modulated fields invoked are either high-frequency electromagnetic fields[12–20] or time-modulated potentials.[21–25] A number of theoretical approaches have been developed to explore quantum transport under such time-modulated fields. The WKB approximation was employed in the study of photovoltaic effect[12] and photon-assisted quantum transport.[13] A mode-matching method was developed for δ-profile[21] as well as finite-range-profile time-modulated potentials.[22] Extension of this method to time-dependent field, represented by a vector potential $\vec{A}(t)$, was carried out by either neglecting[15] or including[18] the contribution of the $\vec{A}(t)^2$ term. This mode-matching method was further extended to accommodate spatial inhomogeneity. The time-modulated field is divided into piecewise potentials connected by either transfer matrices[17] or scattering matrices.[23] Recently, this latter approach has been applied to study a mechanism of nonadiabatic quantum pumping.[25] This pumping mechanism is due to resonances resulting from coherent inelastic scattering, which requires simultaneous changes in both the energy and momentum of the traversing electron, by, respectively, $\hbar\Omega$ and $\hbar K$. Here Ω and K characterize, respectively, the temporal and the spatial variation of the modulation field. Encouraged by the success of the time-modulated mode-matching method, we opt to apply the method to the very interesting case of time-modulated quantum dots.

In the absence of a time-modulated field, transmission of electrons through a quantum dot already shows resonance structures. For the case of a weakly coupled dot—a dot in which electrons are separated from the connecting leads by tunneling barriers—the resonance peaks in the transmission are due to the alignment of the incident electron energy with the quasi-bound-state (QBS) levels in the dot.[26–28] Interestingly, QBS's of a similar nature still exist in the case of an open quantum dot—where tunneling barriers between the dot and the lead are absent. These QBS's, again, give rise to resonances in the transmission. However, dip structures, rather than peaks, become the signatures for the resonances.

When acted upon by a time-modulated potential, the transmission of a weakly coupled dot was found to exhibit additional resonance peaks: peaks associated with ac sidebands.[29] This is due to the alignment, albeit shifted by $n\hbar\omega$, of the incident electron energy with the QBS levels in the dot. Other features found in a time-modulated weakly coupled dot are photon-assisted tunneling,[30] electron pumps,[31] and phase breaking.[32]

Recently, an open quantum dot, acted upon by a transversely polarized electromagnetic field, and connected adiabatically to the connecting leads, has been considered.[33,34] The adiabatic dot-lead connections allow an electron mode in the lead to evolve into an electron mode in the dot. Thus, situations occur when an electron in the lower mode in the dot can exit the dot without reflection, while an electron at the same energy, but in a higher mode in the dot, is trapped inside it. As such, intermode transitions between the above two modes in the dot, as induced by the transversely polarized electromagnetic field, were found to lead to giant mesoscopic conductance fluctuations[33] and microwave-induced resonant blocking in a mesoscopic channel.[34]

The adiabaticity of the dot-lead connection holds for large quantum dots. But, as the sizes of the open quantum dot shrink and approach the realm of the Fermi wavelength, the dot-lead connections can no longer remain adiabatic. More recent experimental findings in dc transport in open quantum dots—that transport occurs through individual eigenstates of the corresponding closed dot;[35] and that the conductance oscillations correlate to the recurrence of specific groups of

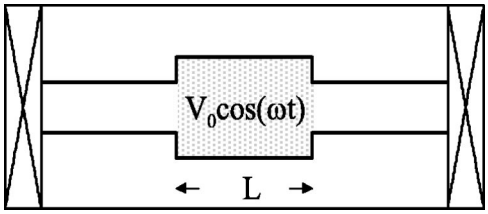

FIG. 1. Schematic illustration of an open quantum dot that is acted upon by a gate-induced time modulation with two leads connecting adiabatically to two end electrodes.

wave function scars in the dot[10]—indicate unequivocally that intermode scattering and backscattering are present, respectively, at the dot-lead connections. The effect of impurity should play no role here because of the high mobility of the sample used in these experiments.

Therefore, in this work, we consider a time-modulated open quantum dot with nonadiabatic dot-lead connections. We calculate the dc conductance G of a time-modulated open quantum dot and the dwell time $\tau_{\rm d}$ of the traversing electron in the dot. We have analyzed the resonance structures in G associated with the time modulation and are able to categorize them according to their respective dynamical processes involved. Of these three resonance types, one is analogous to that found in time-modulated weakly coupled dots. It is associated with the alignment of the incident electron energy with that of the ac sidebands of the QBS's inside the open dot. The second type is associated with the coherent inelastic scattering of the traversing electron into the true bound state in the open dot—bound state whose energy is lower than the threshold energy of the leads. The third type of resonance structures is most unexpected. It is associated with the coherent inelastic scattering of the traversing electron into the QBS in the lead—with energy just beneath the threshold energy of the lead. Also, from the dwell time $\tau_{\rm d}$, we estimate the number of scatterings that occur in the dot as the resonance structures establish themselves. In all, our results demonstrate the potential of establishing quantum transport as a spectroscopic probe for the QBSs and true bound states in the open dot—and possibly in other mesoscopic structures—through the coupling of a time-modulated field to the system.

In Sec. II, we present our theoretical method for the calculation of G and $\tau_{\rm d}$. The numerical results are presented and discussed in Sec. III. Finally, in Sec. IV, we present our conclusions.

II. MODEL AND METHOD

The system under investigation is sketched (top view) in Fig. 1, where the shaded area denotes the region acted upon by a time-modulated potential. The dot we consider has physical parameters typical to that in high mobility two-dimensional electron gas, formed in an AlGaAs-GaAs heterostructure. As such, mobility $\mu_e \sim 10^6$ cm^2/V s, mean free path $l \sim 1$ μm at sufficient low temperatures, and dots with submicron dot sizes would be in the ballistic regime. The Hamiltonian is given by

$$H = -\frac{\hbar^2}{2m}\left[\frac{\partial^2}{\partial x^2}+\frac{\partial^2}{\partial y^2}\right]+V_c(x,y)+V(x,t), \qquad (1)$$

where $V_c(x,y)$ is the confinement potential, chosen to be of hard-wall type, that defines the dot and the leads. It is given by $V_c=0$ if $|y|<W_1/2$ and $|x|>L/2$; $V_c=0$ if $|y|<W_2/2$ and $|x|<L/2$; and $V_c=\infty$ if otherwise. Here W_1, W_2 are, respectively, widths of the lead and the dot. The time-modulated potential

$$V(x,t)=V_0\cos(\omega t)\Theta(L/2-|x|)$$

acts only upon the dot.

For the sake of convenience, the physical quantities that appear in the following equations are dimensionless: with energy unit $E^*=E_F=\hbar^2k_F^2/2m$, wave vector unit $k^*=k_F$, length unit $a^*=1/k_F$, time unit $t^*=\hbar/E_F$, and frequency unit $\omega^*=1/t^*$. The scattering wave function for an electron incident upon the dot from the lth channel in the left lead is of the form

$$\psi_l(x,y,t)=\chi_l(y)e^{ik_l(0)x}e^{-i\mu t}+\sum_{n'}\sum_{m'}\chi_{n'}(y)r_{n'l}(m')\times\exp[-ik_{n'}(m')x-i(\mu+m'\omega)t] \quad \text{if } x<-L/2,$$

$$\psi_l(x,y,t)=\sum_{k'}\phi_{k'}(y)\int d\epsilon[\tilde{A}_{k'l}(\epsilon)e^{i\beta_{k'}(\epsilon)x}+\tilde{B}_{k'l}(\epsilon)e^{-i\beta_{k'}(\epsilon)x}]\times\exp\left[-i\epsilon t-i\frac{V_0}{\omega}\sin\omega t\right] \quad \text{if } |x|<L/2, \qquad (2)$$

$$\psi_l(x,y,t)=\sum_{n'}\sum_{m'}\chi_{n'}(y)t_{n'l}(m')\exp[ik_{n'}(m')x-i(\mu+m'\omega)t] \quad \text{if } x>L/2,$$

where the subscripts n' and k' are the subband indices in, respectively, the leads and the dot, and m' is the sideband index. In addition, $k_l(m')=[\mu+m'\omega-(l\pi/W_1)^2]^{1/2}$ and $\beta_{k'}(m')=[\mu+m'\omega-(k'\pi/W_2)^2]^{1/2}$ denote, respectively, the wave vectors in the lead and the dot. The normalized transverse subband states are $\chi_l(y)=(2/W_1)^{1/2}\sin[l\pi(y/W_1+1/2)]$ and $\phi_{k'}(y)=(2/W_2)^{1/2}\sin[k'\pi(y/W_2+1/2)]$.

The matching of the wave functions at the openings of the dot, and at all times, requires the coefficients in the dot to have the form

$$\tilde{\mathcal{F}}_{k'l}(\epsilon)=\sum_{m'}\mathcal{F}_{k'l}(m')\delta(\epsilon-\mu-m'\omega),$$

where $\tilde{\mathcal{F}}_{k'l}(\epsilon)$ refers to either $\tilde{A}_{k'l}(\epsilon)$ or $\tilde{B}_{k'l}(\epsilon)$. Performing the matching, and after some algebra, we obtain

$$\left[A_{kl}(m)\exp\left(-i\beta_k(m)\frac{L}{2}\right)+B_{kl}(m)\exp\left(i\beta_k(m)\frac{L}{2}\right)\right]$$
$$=\sum_{n'}\sum_{m'}J_{m'-m}\left(\frac{V_0}{\omega}\right)\left[a_{lk}\exp\left(-ik_l(m')\frac{L}{2}\right)\delta_{n'l}\delta_{m'0}+a_{n'k}r_{n'l}(m')\exp\left(ik_{n'}(m')\frac{L}{2}\right)\right], \tag{3}$$

$$\left[A_{kl}(m)\exp\left(i\beta_k(m)\frac{L}{2}\right)+B_{kl}(m)\exp\left(-i\beta_k(m)\frac{L}{2}\right)\right]$$
$$=\sum_{n'}\sum_{m'}J_{m'-m}\left(\frac{V_0}{\omega}\right)\left[a_{n'k}t_{n'l}(m')\exp\left(ik_{n'}(m')\frac{L}{2}\right)\right], \tag{4}$$

$$\sum_{k'}a_{nk'}\beta_{k'}(m)\left[A_{k'l}(m)\exp\left(-i\beta_{k'}(m)\frac{L}{2}\right)-B_{k'l}(m)\exp\left(i\beta_{k'}(m)\frac{L}{2}\right)\right]$$
$$=\sum_{m'}J_{m'-m}\left(\frac{V_0}{\omega}\right)k_n(m')\left[\delta_{nl}\delta_{m'0}\exp\left(-ik_l(m')\frac{L}{2}\right)-r_{nl}(m')\exp\left(ik_{n'}(m')\frac{L}{2}\right)\right], \tag{5}$$

and

$$\sum_{k'}a_{nk'}\beta_{k'}(m)\left[A_{k'l}(m)\exp\left(i\beta_{k'}(m)\frac{L}{2}\right)-B_{k'l}(m)\exp\left(-i\beta_{k'}(m)\frac{L}{2}\right)\right]$$
$$=\sum_{m'}J_{m'-m}\left(\frac{V_0}{\omega}\right)k_n(m')t_{nl}(m')\exp\left(ik_n(m')\frac{L}{2}\right), \tag{6}$$

where Eqs. (5) and (6) are obtained from matching the derivatives of the wave functions. The overlapping integral a_{lk} of the transverse subband states is given by

$$a_{lk}=\int_{-W_1/2}^{W_1/2}\chi_l(y)\phi_k(y)dy \tag{7}$$

and the identity $\exp(iz\sin\omega t)=\Sigma_p J_p(z)\exp(ip\omega t)$ has been invoked. We have solved Eqs. (3)–(6) for the coefficients $A_{kl}(m)$, $B_{kl}(m)$, $r_{n'l}(m')$ and $t_{n'l}(m')$. Furthermore, we note that the sole appearance of V_0 in Eqs. (3)–(6) is in the form V_0/ω and as an argument of the Bessel functions J_m. This shows a general trend that the effect of the time-modulated potential decreases with the raising of the frequency ω.

In the low drain-source bias regime, the dc conductance is given by

$$G=\frac{2e^2}{h}\sum_{l=1}^{N}T_l, \tag{8}$$

where N denotes the number of propagating channels in the leads. The current transmission coefficient T_l for an electron incident from the lth channel in the lead is

$$T_l=\sum_{n'}\sum_{m'}\frac{k_{n'}(m')}{k_l(0)}|t_{n'l}(m')|^2. \tag{9}$$

The current reflection coefficient R_l has a similar form and the current conservation condition $T_l+R_l=1$ is used to check on our numerical accuracy.

The stationary dwell time within one-dimensional system was well defined.[36] However, in a multichannel system, such as open quantum dots, we should consider not only the probability of finding the particle in the dot, but also that due to evanescent states in the vicinity of the dot. Hence, we define the dwell time as

$$\tau_d=\frac{\int\int_{\mathcal{A}'}\langle|\psi(x,y,t)|^2\rangle_{\text{t.a.}}dxdy}{\int dy j_{\text{inc}}}, \tag{10}$$

where j_{inc} denotes the incident electron flux. The subscript t.a. denotes time average. Here we note that the integral in the numerator and its region of interest $\mathcal{A}'$ include not only the region inside the quantum dot (region II), but also the evanescent modes on both the left-hand side (region I) and the right-hand side (region III) of the dot. Hence, the time-averaged probability density in the numerator of Eq. (10) can be separated into three integrals, expressed explicitly as

$$\int\int_{\text{I}}dxdy\langle|\psi(x,y,t)|^2\rangle_{\text{t.a.}}=\int_{-\infty}^{-L/2}dx\sum_{n'}\sum_{m'}|r_{n'l}(m')|^2e^{2\kappa_{n'}(m')x}, \tag{11}$$

$$\int\int_{\text{II}}dxdy\langle|\psi(x,y,t)|^2\rangle_{\text{t.a.}}=\int_{-L/2}^{L/2}dx\sum_{k'}\sum_{m'}\{A_{k'l}(m')A^*_{k'l}(m')\exp[i(\beta_{k'}(m')-\beta^*_{k'}(m'))x]$$
$$+B_{k'l}(m')B^*_{k'l}(m')e^{-i(\beta_{k'}(m')-\beta^*_{k'}(m'))x}+2\text{Re}[A_{k'l}(m')B^*_{k'l}(m')e^{i(\beta_{k'}(m')+\beta^*_{k'}(m'))x}]\}, \tag{12}$$

and

$$\int \int_{\mathrm{III}} dx dy \langle |\psi(x,y,t)|^2 \rangle_{\mathrm{t.a.}} = \int_{L/2}^{\infty} dx \sum_{n'} \sum_{m'} |t_{n'l}(m')|^2 \exp[-2\kappa_{n'}(m')x], \tag{13}$$

where the indices n' and m' in the summation for regions I and III include only the evanescent waves, and $\kappa_{n'}(m) = -ik_{n'}(m)$. Substituting Eqs. (11)–(13) into Eq. (10), we obtain the average dwell time of electrons in the open quantum dot system.

III. RESULTS AND DISCUSSION

In this section, we present our numerical examples for exploring the time-modulated effects on the quantum transport in open quantum dots—the conductance and the dwell time versus the incident electron energy μ. In the following, we choose energy unit $E^* = 9$ meV, length unit $a^* = 8$ nm, unit of angular frequency $\omega^* = 13.6$ T rad/s, and the effective mass $m^* = 0.067 m_e$, where m_e is the free electron mass of an electron. The geometric parameters are chosen such that the width $W_1 = 10(\cong 80$ nm) for the leads, and the width $W_2 = 20(\cong 160$ nm) and the length $L = 30(\cong 240$ nm) for the open quantum dot, which is typical for current experimental fabrication. It is convenient to define $X^2 \equiv \mu/\varepsilon_1$ where $\varepsilon_1 = (\pi/W_1)^2$ is the first transverse subband level in the leads. Then the integral values of X stand for the number of occupied subbands in the leads.

In the absence of time modulation, the quantum states of the open quantum dot associate closely with the bound states of the corresponding closed dot with the same geometry. For a closed dot with length L and width W_2, the bound-state energy $E_{\mathrm{b.s.}} = (n_x \pi/L)^2 + (n_y \pi/W_2)^2$ is labeled by a pair of quantum number (n_x, n_y). Then we may obtain the rescaled bound-state levels $\underline{E}(n_x, n_y) \equiv E_{\mathrm{b.s.}}/\varepsilon_1 = n_x^2/9 + n_y^2/4$ inside the closed dot. For an open dot, the energy spectrum consists of both true bound states and QBS's corresponding either to electrons with energy μ less than or higher than the threshold energy ε_1 in the lead. As such, there are only two possible true bound states in the open dot: $E_{B1} \simeq \underline{E}(1,1) = 0.361$ and $E_{B2} \simeq \underline{E}(2,1) = 0.694$.

In Fig. 2, the conductance characteristic is studied as a function of incident electron energy: (a) in the absence of time modulation, as a comparative reference and (b)–(d) in the presence of time modulation with angular frequencies $\omega/\varepsilon_1 = 0.1$, 0.3, and 0.5, respectively, which also correspond to frequencies $f = \omega/2\pi \simeq 21.4$, 64.2, and 107 GHz. This frequency range is typical for current experiments.[37] In addition, the modulation amplitude is chosen to be $V_0 = 0.1\varepsilon_1$ ($\simeq 0.09$ meV). There are three dip structures common to all four plots. These dip structures occur at energies $\mu/\varepsilon_1 = 2.364(E_{Q1})$, $2.672(E_{Q2})$, and $3.208(E_{Q3})$. These are associated with the alignment of the incident electron energy with that of the QBS levels inside the open dot, as is indicated by the open triangle symbols locating the closed dot $\underline{E}(1,3) = 2.361$, $\underline{E}(2,3) = 2.694$, and $\underline{E}(3,3) = 3.250$. The corresponding dwell time of these QBSs are, respectively, $\tau_d \simeq 73.5$, 26.7, and 69.0 ps, as shown in Fig. 3(a). These dwell time peak structures confirm the resonant nature of the states inside the dot.

Another interesting feature in Fig. 2(b) are the side-dip structures around the QBS's E_{Qi}, which are associated with electrons at incident energy μ that are able to make m-photon intersideband transitions into the ith QBS level. The condition is

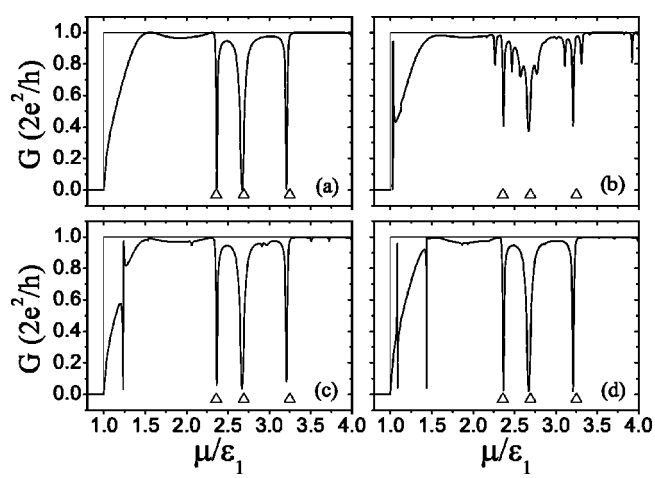

FIG. 2. Energy dependence of the quantum dot conductance G in the lowest subband as a function of incident electron energy μ, in units of ε_1, for cases of (a) no external modulation, (b)–(d) modulation amplitude $V_0 = 0.1\varepsilon_1$, with angular frequencies (b) $\omega = 0.1\varepsilon_1$, (c) $0.3\varepsilon_1$, and (d) $0.5\varepsilon_1$.

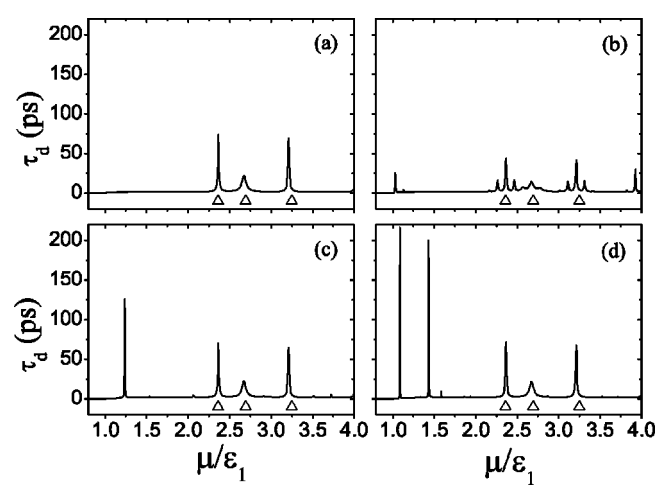

FIG. 3. The dwell time τ_d of the traversing electron is plotted as a function of the incident electron energy μ in units of ε_1. The parameters are the same as in Figs. 2(a)–2(d).

$$\mu + m\hbar\omega = E_{Qi}, \tag{14}$$

where the positive m and negative m indicate, respectively, the absorption and emission of m photons. Hence $m=-1$ side dips are at $\mu/\varepsilon_1=2.465$, 2.770, 3.309; $m=+1$ side dips are at $\mu/\varepsilon_1=2.165$, 2.574, 3.110; and $m=+2$ side dips are at $\mu/\varepsilon_1=2.266$, 3.008. The $m=-2$ process in the vicinity of the E_{Q3} state is barely identified and is at $\mu/\varepsilon_1=3.411$.

Two additional types of intersideband transition mechanisms are found in the low-energy regime in Fig. 2. As is shown in Fig. 2(d), where the frequency $\omega=0.5\varepsilon_1$ is high enough, the electrons with $\mu/\varepsilon_1=1.087$ may emit $\hbar\omega$ and make transitions into E_{B2}—the true bound state in the dot. The electron dwell time of this structure is $\tau_d \cong 216.6$ ps, see Fig. 3(d). In addition, electrons may also emit photons to make transitions into a QBS formed at energy just beneath a subband threshold in the lead. This mechanism is identified to be the fano structures at $\mu/\varepsilon_1=1.028$, 1.233, and 1.435, as shown in Figs. 2(b)–2(d), respectively, where $(\mu-\omega)/\varepsilon_1$ is close to 1 from below. Correspondingly, the dwell times of these structures are $\tau_d \simeq 23.0$, 125.5, and 200.2 ps, see Figs. 3(b)–3(d). More precisely, these structures correspond to electrons that emit $\hbar\omega$ to $\mu/\varepsilon_1=0.93$ and are trapped temporarily to form QBS's in the lead.

To provide further evidence for the above two transition mechanisms, we plot, in Fig. 4, the spatial dependence of the time-averaged probability density. The parameters are chosen to be the same as in Fig. 2(d). When the electron incident at energy $\mu=1.0854\varepsilon_1$, as shown in Fig. 4(a), we see that the time-averaged electron probability concentrates entirely within the dot and is like a (2,1) state. This supports the fact that the electron is trapped in a true bound state in the dot. Second, when the electron incident at energy $\mu=1.4353\varepsilon_1$, the electron probability has long exponential tails extending into the leads. The edges of the dot are at $x=\pm 15$. This demonstrates that the electron has made an intersideband transition, by emitting one photon, into a QBS in the lead whose energy is just below the threshold energy. We have also checked that a similar process can be found even in a time-modulated one-dimensional quantum well connecting to leads. A traversing electron can make intersideband transitions to QBS's in the leads or to true bound states in the well.[38]

To better appreciate the meaning of the dwell time, we define the number of round-trip scatterings, N_{sc}, undertaken by the traversing electron. It is the ratio of the dwell time τ_d to the ballistic time τ_b the electron takes to go between the two dot-openings. The ballistic time for electrons traversing through the quantum dot is simply $\tau_b \sim L/v_e$, where v_e denotes the electron velocity and is given by $v_e=\hbar k_x/m$. We consider the electron incident in the lowest subband and then the electron ballistic time is given by $\tau_b=L/(\mu-\varepsilon_1)^{1/2}$ in units of t^*. Hence, in Fig. 3(d), the main peaks at $\mu/\varepsilon_1=1.085$, 1.435, 2.365, 2.673, and 3.210 correspond to the ballistic times $\tau_b \simeq 24.0$, 16.1, 6.01, 5.43, and 4.72 ps, respectively. The corresponding τ_d's are, respectively, 216.6, 200.2, 71.8, 21.8, and 67.9. Therefore, we obtain the number of round-trip scatterings, $N_{sc} \equiv \tau_d/2\tau_b \sim 4.5$, 6.2, 6.0, 2.0, and 7.2, respectively. In light of the above analysis, we can see that two round-trip times are already sufficient to form a significant QBS level inside the open dot. The estimation for τ_b could be improved by considering the effective electron velocity in the dot, rather than in the lead. But we expect N_{sc} to remain of the same order of magnitude as shown here. Moreover, the N_{sc} obtained here is the lower bound to any such improved estimation.

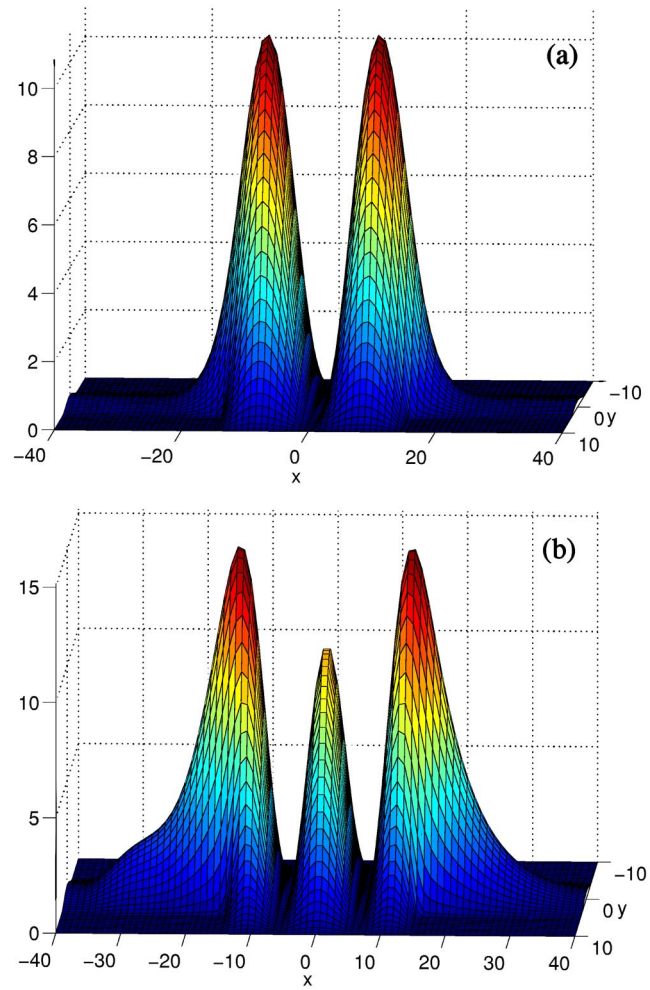

FIG. 4. (color online). The spatial dependence of the time-averaged electron probability density: (a) $\mu=1.0854\varepsilon_1$ and (b) $\mu=1.4353\varepsilon_1$. Other parameters are the same as in Fig. 2(d). The edges of the dot are at $L=\pm 15$.

It is known[22] that the strength of the time-modulated potential depends on the ratio of V_0 to ω. As a result, for a given amplitude V_0, the sideband dip features are suppressed with increase in the modulation frequency ω. This is illustrated in Figs. 2(c) and 2(d). On the other hand, if we fix $V_0/\omega=1$ in Fig. 5, and choose the modulation amplitude to be $V_0/\varepsilon_1=0.05$, 0.1, and 0.2 for Figs. 5(a)–5(c), respectively, we can see the side dips due to $2\hbar\omega$ intersideband processes in all the figures. This assures us that V_0/ω is an important index for photon absorption and emission processes. Furthermore, the QBS levels that associate with a fewer number of round-trip scatterings may be merged with its nearby sidebands, forming a broadened dip structure: such as the wide-dip structure at $\mu/\varepsilon_1=2.672$ in Fig. 5(a). In the

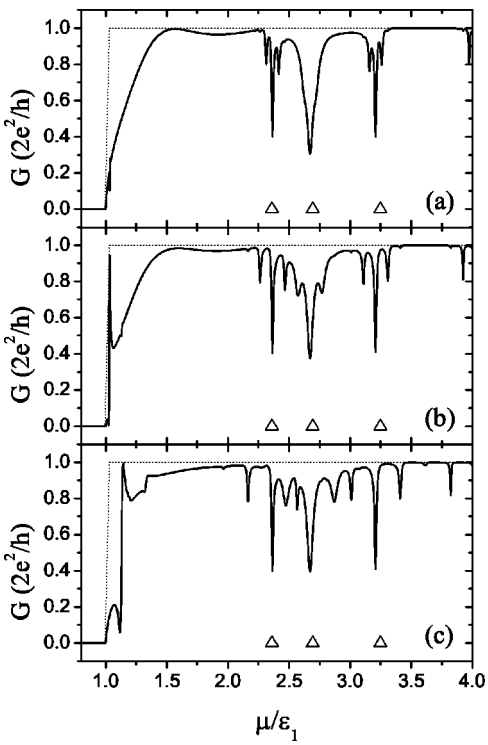

FIG. 5. Conductance is plotted as a function of electron energy μ for a fixed $V_0/\omega=1.0$. The values of V_0 (or ω) are (a) $0.05\varepsilon_1$, (b) $0.1\varepsilon_1$, and (c) $0.2\varepsilon_1$, respectively.

low-energy regime, again, electrons are able to undertake one-photon (or two-photon) emission processes into a subband threshold in the lead. This one-(or two-)photon mechanism is demonstrated by small dip structures in G at $\mu/\varepsilon_1=1.024$ (or 1.129) in Fig. 5(b) and $\mu/\varepsilon_1=1.118$ (or 1.317) in Fig. 5(c).

To conclude this section, we note in passing that despite of wide dot openings, electrons traversing through the dot are still effectively mediated by just a few bound states of the corresponding closed dot structure. Our results show that the conductance spectra for a time-modulated open dot show more intersideband structures than those associated with the bound states of the corresponding close dot. We believe that these mechanisms should find their way of manifestation in the time-modulated phenomena of other nanostructures.

IV. CONCLUSIONS

In this work we have extended the time-dependent mode matching approach to the study of quantum transport in open quantum dot systems. We have calculated the conductance, the dwell time, and the spatial distribution of the electron probability and their dependence on the modulation amplitudes and frequencies.

In conclusion, we have shown three types of coherent inelastic scatterings in a time-modulated open quantum dot. We have demonstrated the potential of establishing quantum transport as a spectroscopic probe for the QBS's and true bound states in an open dot through the coupling of a time-modulated field to the system.

ACKNOWLEDGMENTS

The authors wish to acknowledge the National Science Council of the Republic of China for financially supporting this research under Grants Nos. NSC90(91)-2119-M-007-004 (NCTS), NSC90-2112-M-262-001 (CST), and NSC90-2112-M-009-044 (CSC). Computational facilities supported by the National Center for High-Performance Computing are gratefully acknowledged.

[1] C.M. Marcus, A.J. Rimberg, R.M. Wetervelt, P.F. Hopkins, and A.C. Gossard, Phys. Rev. Lett. **69**, 506 (1992).
[2] A.M. Chang, H.U. Baranger, L.N. Pfeiffer, and K.W. West, Phys. Rev. Lett. **73**, 2111 (1994).
[3] H.I. Chan, R.M. Clarke, C.M. Marcus, K. Campman, and A.C. Gossard, Phys. Rev. Lett. **74**, 3876 (1995).
[4] M. Persson, J. Pettersson, B. von Sydow, P.E. Lindelof, A. Kristensen, and K.-F. Berggren, Phys. Rev. B **52**, 8921 (1995).
[5] M.W. Keller, A. Mittal, J.W. Sleight, R.G. Wheeler, D.E. Prober, R.N. Sacks, and H. Shrtikmann, Phys. Rev. B **53**, R1693 (1996).
[6] Y. Wang, N. Zhu, and J. Wang, Phys. Rev. B **53**, 16 408 (1996).
[7] R. Akis, D.K. Ferry, and J.P. Bird, Phys. Rev. Lett. **79**, 123 (1997).
[8] I.V. Zozoulenko and T. Lundberg, Phys. Rev. Lett. **81**, 1744 (1998).
[9] R. Akis, D.K. Ferry, and J.P. Bird, Phys. Rev. Lett. **81**, 1745 (1998).
[10] J.P. Bird, R. Akis, D.K. Ferry, D. Vasileska, J. Cooper, Y. Aoyagi, and T. Sugano, Phys. Rev. Lett. **82**, 4691 (1999).
[11] A.P.S. de Moura, Y.-C. Lai, R. Akis, J.P. Bird, and D.K. Ferry, Phys. Rev. Lett. **88**, 236804 (2002).
[12] F. Hekking and Y.V. Nazarov, Phys. Rev. B **44**, 11 506 (1991).
[13] S. Feng and Q. Hu, Phys. Rev. B **48**, 5354 (1993).
[14] L.Y. Gorelik, A. Grincwajg, V.Z. Kleiner, R.I. Shekhter, and M. Jonson, Phys. Rev. Lett. **73**, 2260 (1994).
[15] F.A. Maaø and L.Y. Gorelik, Phys. Rev. B **53**, 15 885 (1996).
[16] C.S. Chu and C.S. Tang, Solid State Commun. **97**, 119 (1996).
[17] M. Wagner and W. Zwerger, Phys. Rev. B **55**, R10 217 (1997).
[18] C.S. Tang and C.S. Chu, Phys. Rev. B **60**, 1830 (1999).
[19] Wenjun Li and L.E. Reichl, Phys. Rev. B **62**, 8269 (2000).
[20] C.S. Tang and C.S. Chu, Physica B **292**, 127 (2000).
[21] P.F. Bagwell and R.K. Lake, Phys. Rev. B **46**, 15 329 (1992).
[22] C.S. Tang and C.S. Chu, Phys. Rev. B **53**, 4838 (1996).
[23] C.S. Tang and C.S. Chu, Physica B **254**, 178 (1998).
[24] Wenjun Li and L.E. Reichl, Phys. Rev. B **60**, 15 732 (1999).
[25] C.S. Tang and C.S. Chu, Solid State Commun. **120**, 353 (2001).
[26] J. Wang and H. Guo, Appl. Phys. Lett. **60**, 654 (1992).
[27] S. Tarucha, D.G. Austing, T. Honda, R.J. van der Hage, and L.P. Kouwenhoven, Phys. Rev. Lett. **77**, 3613 (1996).

[28] L.P. Kouwenhoven *et al.*, in *Mesoscopic Electron Transport, Vol. 345 of Proceeding of a NATO Advanced Studies Institute, Series E: Applied Sciences*, edited by L.L. Sohn, L.P. Kouwenhoven, and G. Schön (Kluwer, Dordrecht, 1997).
[29] T.H. Oosterkamp, L.P. Kouwenhoven, A.E.A. Kooten, N.C. van der Vaart, and C.J.P.M. Harmans, Phys. Rev. Lett. **78**, 1536 (1997).
[30] T. Christen and M. Büttiker, Phys. Rev. B **53**, 2064 (1996).
[31] L.J. Geerlings, V.F. Anderegg, P.A.M. Holweg, J.E. Mooij, H. Pothier, D. Esteve, C. Urbina, and M.H. Devoret, Phys. Rev. Lett. **64**, 2691 (1990).
[32] M.P. Amatram and S. Datta, Phys. Rev. B **51**, 7632 (1995).
[33] L.Y. Gorelik, F.A. Maaø, R.I. Shekhter, and M. Jonson, Phys. Rev. Lett. **78**, 3169 (1997).
[34] S. Blom and L.Y. Gorelik, Phys. Rev. B **64**, 045320 (2001).
[35] I.V. Zozoulenko, A.S. Sachrajda, C. Gould, K.-F. Berggrem, P. Zawadzki, Y. Feng, and Z. Wasilewski, Phys. Rev. Lett. **83**, 1838 (1999).
[36] F.T. Smith, Phys. Rev. **118**, 349 (1960).
[37] H. Qin, F. Simmel, R.H. Blick, J.P. Kotthaus, W. Wegscheider, and M. Bichler, Phys. Rev. B **63**, 035320 (2001).
[38] C.S. Tang and C.S. Chu (unpublished).